Electrochimica Acta 385 (2021) 138306

Contents lists available at ScienceDirect

Electrochimica Acta

journal homepage: www.elsevier.com/locate/electacta

Nanoporous Pd-Cu thin films as highly active and durable catalysts for oxygen reduction in alkaline media

Yunxiang Xie, Can Li, Ezer Castillo, Jiye Fang, Nikolay Dimitrov*

Department of Chemistry, State University of New York at Binghamton, PO Box 6000, Binghamton, NY 13902, United States

ARTICLE INFO

Article history:
Received 7 January 2021
Revised 31 March 2021
Accepted 31 March 2021
Available online 8 April 2021

Keywords:
Nanoporous metals
PdCu alloy
Alkaline media
Oxygen reduction reaction
De-alloying

ABSTRACT

A facile electrochemical etching approach was developed and implemented to enhance the electrocatalytic performance of Pd-Cu films for oxygen reduction reaction (ORR) in alkaline media. The nanoporous (np) Pd-Cu was synthesized through electrochemical de-alloying of pre-deposited Pd-Cu films. Scanning electron microscopy (SEM) with energy dispersive spectroscopy was employed to confirm the residual amount of Cu in the np structure. The accordingly prepared np catalysts showed excellent ORR activity up to 1.11 A/mg_{Pd} at a potential of 0.9 V vs. RHE which is around 22-times and 6.2-times higher than that of a plain Pd film and commercial Pd/C catalyst, respectively. The ORR activity enhancement is attributed to the unique porous structure, large Pd surface area, and modified electronic structure of Pd with residual Cu as confirmed by the SEM, hydrogen underpotential deposition, and CO stripping characterizations. The np Pd-Cu catalyst also showed excellent durability which is manifested by a negligible decrease in the half-wave potential (4 mV negative shift) after 10,000 potential cycles in alkaline media. These findings provide insights into the rational design of an electrocatalyst's structure utilizing an electrochemical de-alloying method to achieve high atomic utilization and improved catalytic performance.

1. Introduction

Fuel cells have attracted a great deal of attention as potential power sources for automotive and portable devices due to their high energy density and high conversion efficiency [1–3]. Recently, alkaline fuel cells have emerged as one of the most promising energy sources because of their operation in a less corrosive environment and the relatively faster oxygen reduction reaction (ORR) kinetics compared with proton-exchange membrane fuel cells [4–6]. With that said, the ORR kinetics is still generally sluggish in alkaline media so there is a pressing need for the development of a new generation of more efficient, low-cost, and durable ORR electrocatalysts [7,8]. To that end, the research effort has been focused on alloying Pt or Pd with transition metal(s) aimed at overall cost reduction and altering the electronic structure [8]. Previous studies have shown that Pd-based electrocatalysts possess a higher activity and better durability in comparison with commercial Pt/C [9–11]. Among those Pd-based catalysts, the Pd-Cu binary system exhibits an excellent catalytic performance which has been attributed to an optimum d-band center position of the alloyed Pd [12,13] and the sufficient thermodynamic stability of Pd-Cu alloys in alkaline media [14,15]. These good catalytic properties render the Pd-Cu system a promising candidate for an ORR electrocatalyst in alkaline media.

Electrochemical methods (electrodeposition and electrochemical de-alloying) have been largely employed in the process of synthesis and/or modification of electrocatalysts owing to their flexibility and ease of use. For instance, the Pd-Bi catalysts with high ORR activity were synthesized by electrodeposition [16]. Electrochemical de-alloying of Pd-Ni nanoparticles was found to improve their catalytic performance [17]. Our work emphasized electrodeposition and subsequent de-alloying for the synthesis of nanoporous (np) films with tunable composition and structure aimed at applications in energy conversion [18,19]. Most of the development effort for the synthesis of Pd-Cu ORR electrocatalysts has been focused on the use of nanoparticle systems [14,20]. Recently, Pd-Cu nanostructures developed by galvanic displacement of Cu layer with Pd were studied as ORR catalysts in alkaline media [21]. To the best of our knowledge, continuous np Pd-Cu films, prepared via a co-deposition/de-alloying technique, for ORR studies in alkaline media has not been reported. Overall, exploring the np Pd-Cu films as catalysts for ORR in alkaline media is worthwhile because of (i) their high surface that is comparable to that of nanoparticles [22–24], and (ii) their ability to retain Cu in a controllable manner [15,20,21] during the de-alloying step. The latter feature could also enable tunability of the Pd electronic structure and could thus benefit the ORR catalytic activity [25,26].

* Corresponding author.
E-mail address: dimitrov@binghamton.edu (N. Dimitrov).

https://doi.org/10.1016/j.electacta.2021.138306
0013-4686/

In this work, a facile method comprising of electrochemical deposition and subsequent de-alloying was employed to synthesize an np Pd-Cu catalyst. Binary Pd-Cu alloy films with different compositions were firstly prepared by electrodeposition on glassy carbon (GC) electrodes and then tested for ORR activity as the reference. Scanning electron microscopy with energy dispersive spectroscopy (SEM-EDS) was used to confirm the composition of accordingly prepared Pd-Cu films. Following all that, the Cu was then selectively etched (de-alloyed) by anodic potential scan between 0.1 V and 1.0 V vs. Cu/Cu^{2+} from the Pd-Cu films with high Cu content (more than 50% Cu). The accordingly synthesized electrocatalysts after de-alloying are denoted as np Pd-Cu. SEM and EDS were used for morphological and compositional analysis of np Pd-Cu, respectively. The electrochemical characterization methods such as hydrogen underpotential deposition (H_{UPD}) and CO stripping were employed to probe the electrochemical surface area (ECSA) and electronic structure of Pd, respectively. Linear sweep voltammetry (LSV) and cyclic voltammetry (CV) were employed for ORR activity and durability tests.

2. Experimental

2.1. Electrode preparation

GC rotating-disk electrodes (RDEs; Pine Instruments) with a 5.0 mm diameter (surface area of 0.196 cm^2) were used as working electrodes (WEs) for electrochemical characterization and measurements. The WEs were first mechanically polished using 1 μm alumina slurry (Buehler) followed by rinsing with Barnstead Nanopure® water (18.2 MΩ cm). Then, the WEs were immersed in a warm solution containing concentrated HNO_3 to remove trace contaminants followed by another rinsing with Barnstead Nanopure® water. Glassy carbon WEs, subjected to the same preparation routines and employed for the GC RDE work, were used also as carriers of electrocatalysts that were being subjected to SEM and EDS characterizations.

2.2. Pd-Cu film, nanoporous structure fabrication and Pd/C ink preparation

The Pd-Cu thin film on the GC RDE surface was prepared by overpotential co-deposition of Pd and Cu in a three-electrode cell at −0.70V versus a saturated mercury-mercurous sulfate (MSE) reference electrode (RE). A total deposition charge of 50 mC/cm^2 was targeted in all experiments. A Pt wire was used as the counter electrode (CE) for all the electrochemical experiments. The solution for Pd-Cu film deposition contained X mM $Cu(ClO_4)_2$ (Alfa Aesar, 99.999%), Y mM Na_2PdCl_4 (STREM Chemical, 99%), 50 mM HCl (J.T.Baker, 36.5−38.0%), and 100 mM $NaClO_4$ (GFS Chemicals, 98%). The composition of the prepared Pd-Cu film was controlled by tuning the X and Y. The details are as follow: *X*= 0.80 mM, *Y*= 0.18 mM ($Pd_{0.18}Cu_{0.82}$); *X*= 0.80 mM, *Y*= 0.80 mM ($Pd_{0.50}Cu_{0.50}$); *X*= 0.18 mM, *Y*= 1.44 mM ($Pd_{0.89}Cu_{0.11}$). The plain Pd film was prepared under the same condition without adding $Cu(ClO_4)_2$. After the deposition, the Pd-Cu film was rinsed thoroughly with Barnstead Nanopure® water and then dried gently with ultra-high purity N_2. Anodic LSV was used to fabricate nanoporous Pd-Cu by selective removal of Cu from the as-deposited Pd-Cu film. These experiments were carried out in a solution containing 1 mM $CuSO_4$ (J.T. Baker, 99.8%) and 100 mM $HClO_4$. A Cu wire was used as the pseudo-RE, 0.250 V vs standard hydrogen electrode (SHE), in the de-alloying experiments. The de-alloying protocol was administered through an anodic potential scan from 0.10 to 1.00 V versus Cu/Cu^{2+} at a scan rate of 1 mV/s, generating composition-controlled electrocatalyst films, denoted as the “porous film”. A PAR model 273 Potentiostat/Galvanostat operated by a PC equipped with CorrWare® 3.5h software was used for the overpotential co-deposition and anodic LSV. The commercial Pd/C catalyst was used for the ORR test for comparison. The preparation of the Pd/C nanoparticle ink that is then coated on the testing electrode, involves mixing of 2.0 mg of Pd/C (10 wt%, Sigma-Aldrich) with 0.5 mL of 1-propanol (Sigma-Aldrich), 0.5 mL of Nanopure® water (18.2 MΩ•cm), and 40.0 µL of Nafion solution (5 wt%, Sigma-Aldrich) for at least 30 min under ultrasonication until a uniform mixture was generated. Then, 27.5 µL of the fresh Pd/C ink (2.0 mg/ml) was dropped on a GC electrode (5 mm in diameter). The electrode was finally dried at room temperature naturally before any electrochemical measurement.

2.3. Structure and composition characterization

SEM (Zeiss Supra 55 VP) coupled with in-lens and SE2 detectors, operated at an accelerating voltage from 5 to 15 keV, was employed for the structural characterization of all porous films using a working distance between 3 and 6 mm. The elemental composition of the synthesized Pd-Cu films and np Pd-Cu layers was determined by SEM equipped with the EDS instrument and operated at an accelerating voltage of 15 kV and a working distance of 8.5 mm.

2.4. Electrochemical characterization

The ECSA of Pd was estimated by CV scanning at 50 mV/s in a 0.5 M H_2SO_4 (GFS Chemical, redistilled 95−98%) solution over the potential range between −0.62 and 0.10 V vs. MSE. We employed a Pine Instruments model AFCBP Bipontentiostat interfaced with a PC through Aftermath Data Organizer software. All solutions were purged using ultrahigh purity N_2 for at least 30 min before use. The ECSA of Pd was calculated by integrating the area of H_{UPD} over the potential range from -0.62V to -0.40V vs. MSE. The equation, $A_{Pd-H\ UPD} = Q_{H\ UPD}\ (\mu C)/210 \mu C\ cm^{-2}$, was used to calculate the ECSA of Pd [27]. The carbon monoxide (CO) stripping technique was used to probe the ECSA of Pd, comparatively with the H_{UPD} method, and to also probe the electronic structure of Pd. For those measurements, the as-prepared catalysts were immersed into a solution containing 0.5 M H_2SO_4, and then the solution was purged for 10 min with CO gas while a potential of −0.61 V vs. MSE was applied. Next, the solution was purged with ultra-high purity N_2 for 20 min to eliminate any traces of CO in the solution. Finally, a CV scan from −0.62 to 0.55 V vs. MSE at 50 mV/s was applied to strip the adsorbed CO. A second potential cycle was applied after the first stripping one to ensure the complete CO adlayer removal from the surface. The CO stripping charge (in 0.5M H_2SO_4) was calculated by integrating the area between the 1st and 2nd cycle, and the following equation was used to calculate the ECSA of Pd: $A_{Pd-CO\ stripping} = Q_{CO\ Stripping}(\mu C)/420\ \mu C\ cm^{-2}$ [28]. The ECSA of Pd determined by the CO stripping technique (in 0.5M H_2SO_4) was used to calculate the specific activity of prepared electrocatalysts. The H_{UPD} and CO stripping were also conducted in the alkaline media (0.1M KOH) for the sake of completeness of the study. The experimental conditions were similar to the one in an acidic environment, only the potential range was adjusted to account for the pH difference. More specifically, for the H_{UPD}, the CV was scanned at potential range between −1.35 and -0.25 V vs. MSE; for the CO stripping, the solution (0.1M KOH) was purged for 10 min with CO gas first, followed by N_2 gas purging for another 20 min while a potential of −1.32 V vs. MSE was applied and then CV scan from −1.35 to -0.35 V vs. MSE at 50 mV/s was applied to strip the adsorbed CO. A Gamry Interface 1000 Potentiostat/Galvanostat/ZRA operated by a PC equipped with a Gamry framework was used for control of the CO stripping test.

2.5. ORR studies

A PAR model 273 Potentiostat/Galvanostat operated by a PC equipped with CorrWare® 3.5h software was used for all ORR tests. The experiments were conducted in a conventional three-electrode cell with MSE as the RE. The MSE has a potential of 0.65 V vs. SHE. No iR compensation was applied in these experiments for the sake of the most conservative catalytic performance evaluation. The potential value was converted to RHE as following (Eq. (1)):

$$E(V,\ RHE) = E(V\ vs.\ MSE) + 0.0592\ pH + 0.650\ V \quad (1)$$

The ORR performance was evaluated by the anodic LSV with a catalyst deposited on the GC-RDE carrier at a scan rate of 10 mV/s and rotation rate of 1600 rpm in an oxygen (O_2) saturated 0.1 M KOH solution. The kinetic current (j_k) was calculated by using the Koutecky–Levich (K–L) equation (Eq. (2)) [29]:

$$1/j = 1/j_k + 1/j_d \quad (2)$$

The number of transferred electrons was calculated by using the Levich Eq. (3) [29]:

$$j_d = 0.2nF(D_{O2})^{2/3}\nu^{-1/6}\omega^{1/2}C_{O2} \quad (3)$$

Here, n is the number of electrons transferred per O_2, F is the Faraday constant (96,485 C/mol), D_{O2} is the diffusion coefficient of O_2 in the electrolyte (1.9 Å~ 10^{-5} cm^2/s), ν is the kinetic viscosity of 0.1 M KOH (0.01 cm^2/s), ω is the rotation speed in rpm, and C_{O2} is the concentration of O_2 in 0.1 M KOH (1.2×10^{-6} mol/cm^3) [30]. An accelerated durability test (ADT) was performed between 0.6 and 1.0 V (vs. RHE) at a scan rate of 100 mV/s for 10,000 cycles.

3. Results and discussion

3.1. Characterization of Pd-Cu Film

The Pd-Cu films with different Pd:Cu contents were synthesized by electrodeposition at constant potential on a GC substrate, with a total deposition charge density of 50 mC/cm^2. The morphology of Pd and Pd-Cu films was characterized by SEM as shown in Fig. 1. The overall surface is generally smooth, and the layer-continuity was achieved by the coalescence of an initially nucleated high-density array of small metallic clusters. Fig. 1**B** presents the morphology of Pd-Cu with higher Pd content which features a continuous surface similar to the Pd film (Fig. 1**A**). With the increase of Cu content in Pd-Cu film, the overall surface morphology still suggests a layer grown after initial dense nucleation. The bulk composition of prepared films was determined by SEM-EDS and the results are summarized in **Table 1**. The SEM-EDS spectra are presented in **SI, Fig. S1**. By comparing the results from the SEM-EDS and the corresponding atomic ratio from each precursor solution, one can conclude that the SEM-EDS composition is close to the Pd:Cu solution ratio. This indicates the composition is generally tunable by controlling the $Cu(ClO_4)_2$ and Na_2PdCl_4 concentrations in the precursor solution. All Pd-Cu films used in this work are labeled by the precursor solution ratio in the text. Also, the Pd:Cu compositions that are used for ORR mass activity calculation are estimated using the SEM-EDS results.

Table 1
Summary of Pd-Cu film composition measured by EDS.

Pd-Cu film (precursor solution ratio)	Pd content (SEM-EDS)	Cu content (SEM-EDS)
$Pd_{0.89}Cu_{0.11}$	84.5±2.5	15.5±2.5
$Pd_{0.50}Cu_{0.50}$	50.9±3.0	49.1±3.0
$Pd_{0.18}Cu_{0.82}$	16.6±2.9	83.4±2.9

3.2. Cu electrochemical etching and nanoporous Pd-Cu formation

The prepared films ($Pd_{0.18}Cu_{0.82}$ and $Pd_{0.50}Cu_{0.50}$) were electrochemically de-alloyed for selective Cu removal. Owing to the retention of some Cu, the de-alloying leads to the formation of np Pd-Cu films that are enriched in Pd in comparison with the precursor alloys. The SI **Fig. S2** shows the Cu stripping curve of $Pd_{0.18}Cu_{0.82}$ and

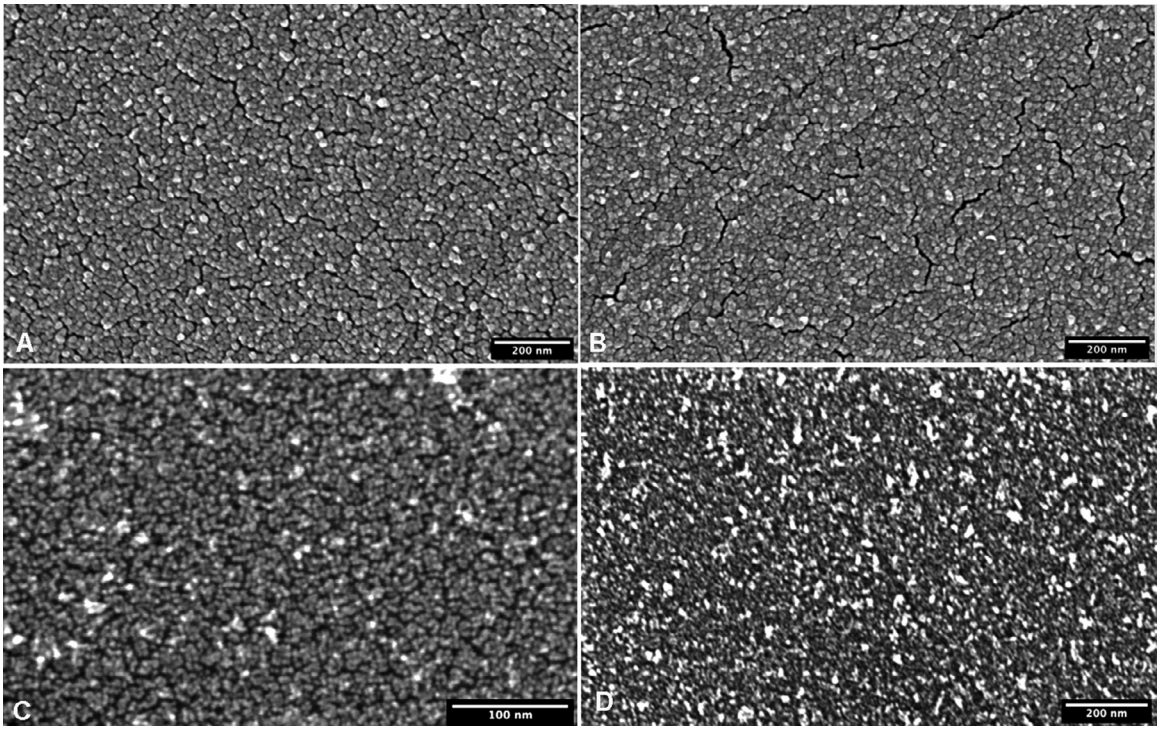

Fig. 1. SEM images of precursor thin film of (A)Pd at 200kx, (B)$Pd_{0.89}Cu_{0.11}$ at 200kx, (C) $Pd_{0.50}Cu_{0.50}$ at 500kx, (D) $Pd_{0.18}Cu_{0.82}$ at 210 kx.

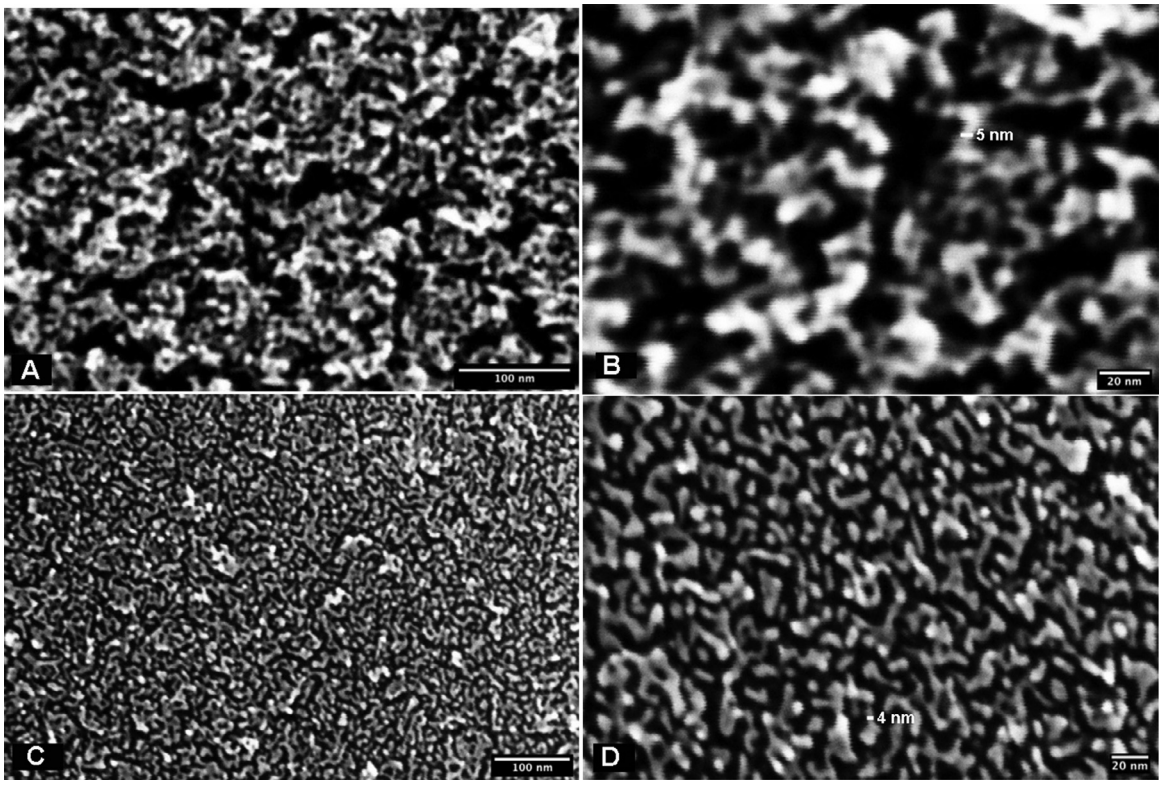

Fig. 2. SEM images of np $Pd_{0.37}Cu_{0.63}$ (A at 576 kx and B at 1270 kx) and np $Pd_{0.65}Cu_{0.35}$ (C at 388 kx and D at 856 kx).

Table 2
Comparison of Cu electrodeposition and stripping charge.

Pd-Cu precursor solution ratio	Precursor Cu Deposition *Total Charge (mC)*	Selective Cu stripping *Total Charge (mC)*
$Pd_{0.18}Cu_{0.82}$	8.10	4.77
$Pd_{0.50}Cu_{0.50}$	4.40	2.37

Table 3
Summary of np Pd-Cu composition measured by EDS.

Pd-Cu film (precursor solution ratio)	Pd content after de-alloying (SEM-EDS)	Cu content after de-alloying (SEM-EDS)
$Pd_{0.18}Cu_{0.82}$	37.2±3.6	62.8±3.6
$Pd_{0.50}Cu_{0.50}$	65.3±1.3	34.7±1.3

$Pd_{0.50}Cu_{0.50}$ films. It could be observed that there are two stripping peaks (at 0.2 V and 0.6 V vs. Cu/Cu^{2+}) which correspond to two different Pd-Cu phases. The high potential (0.6 V vs. Cu/Cu^{2+}) for Cu etching indicates the Pd could considerably stabilize Cu making it less prone to dissolution [31]. As expected, substantially more Cu was being etched during $Pd_{0.18}Cu_{0.82}$ de-alloying (higher original Cu content). The overall Cu stripping (anodic) charge is less than the total deposition charge of Cu as shown in **Table 2**. This indicates that a certain amount of Cu remains entrapped in the np films [18].

The SEM and SEM-EDS were employed to investigate the morphology and composition, respectively, of accordingly prepared np Pd-Cu films. The EDS results (presented in **Table 3** and **SI Fig. S3**) show that the composition of np films is $Pd_{0.37}Cu_{0.63}$ and $Pd_{0.65}Cu_{0.35}$ (de-alloyed from $Pd_{0.18}Cu_{0.82}$ and $Pd_{0.50}Cu_{0.50}$ films, respectively). These films are denoted for future discussion as np $Pd_{0.37}Cu_{0.63}$ and np $Pd_{0.65}Cu_{0.35}$. These results clearly evidence the presence of residual Cu in the as-synthesized np structure. Fig. 2 shows the SEM images at different magnifications of both np $Pd_{0.37}Cu_{0.63}$ and np $Pd_{0.65}Cu_{0.35}$ films. The films exhibit a bi-continuous and interpenetrating solid-void structure [32] with a ligament size of 5-10 nm. The high surface area is due to the very fine porosity length scale of the np structure.

3.3. Electrochemical characterization of nanoporous Pd-Cu

CV was used to characterize the ECSA of Pd film and np Pd-Cu films using underpotential deposition of H (H_{UPD}) as shown in Fig. 3**A**. The red curve represents the H_{UPD} of a Pd film on GC that, similarly to a previous report of H_{UPD} of Pd nanoparticles [33], exhibits three peaks. Peak 1 is related to the bulk H-atoms absorbed in the bulk of the Pd layer, whereas peaks 2 and 3 are related purely to the H_{UPD}. The other two CV curves (green and blue) show a relatively small peak 1 which is due to the strong inhibition of hydrogen adsorption by the Pd alloying with Cu (Pd-Cu) [27]. It should be noted that there are small peaks at potential -0.1 V (cathodic scan) and -0.2 V (anodic scan) for both np $Pd_{0.37}Cu_{0.63}$ and np $Pd_{0.65}Cu_{0.35}$. These peaks are due to the Cu peak of np $Pd_{0.65}Cu_{0.35}$ features a slightly larger area than the np $Pd_{0.37}Cu_{0.63}$ one. It is interesting to observe that the Cu oxidation and reduction could be attributed to the fact that the presence of more Pd (precursor $Pd_{0.50}Cu_{0.50}$) could stabilize the surface Cu from dissolution during the electrochemical etching process **(SI Fig. S2)**. H_{UPD} CV was also performed in alkaline media (0.1M KOH) as presented in **SI Fig. S4A**. It is clear that the overall behavior is similar to that of H_{UPD} in acidic media, with only the potential shifting to more negative values due to the high pH impact. Fig. 3**B** presents a two-cycle CO stripping experiment carried out on films of Pd on GC, np $Pd_{0.65}Cu_{0.35}$, and np $Pd_{0.37}Cu_{0.63}$ which emphasize and confirm the complete CO oxidation taking place in the first cycle. Since the presence of Cu as an alloying element could partially inhibit the H_{UPD} formation, the CO stripping charge (normalized to 420 $\mu C/cm^2$), was exclusively used to determine the ECSA of Pd. **Table 4** summarizes the ECSA (from both H_{UPD} and CO stripping)

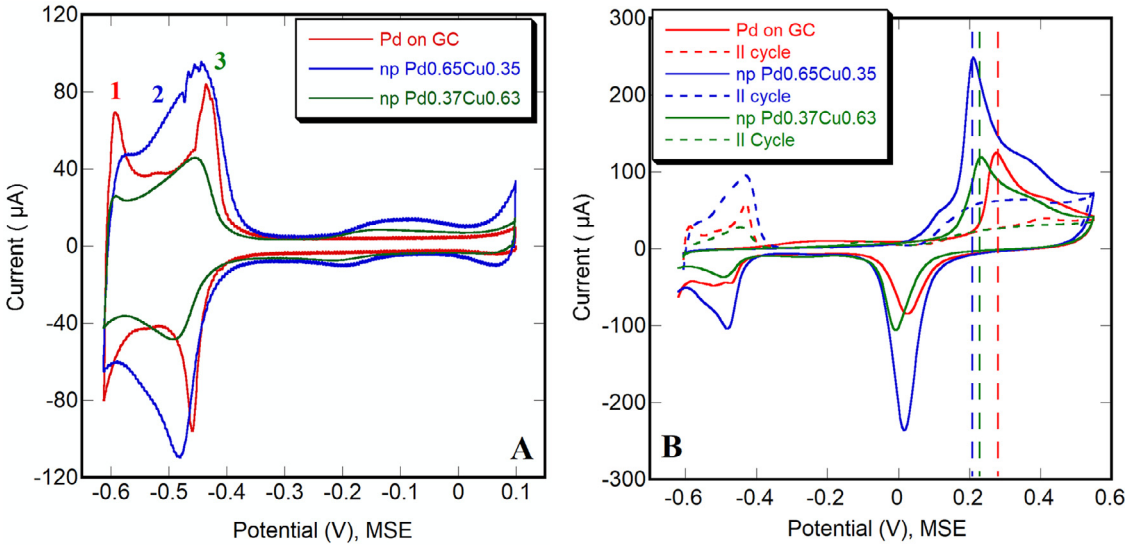

Fig. 3. (A) H_{UPD} curves for Pd on GC, np $Pd_{0.65}Cu_{0.35}$ and np $Pd_{0.37}Cu_{0.63}$ in 0.5 M H_2SO_4 at 50 mV/s (B) CO stripping curves for Pd on GC, np $Pd_{0.65}Cu_{0.35}$ and np $Pd_{0.37}Cu_{0.63}$ in 0.5 M H_2SO_4 at 50 mV/s.

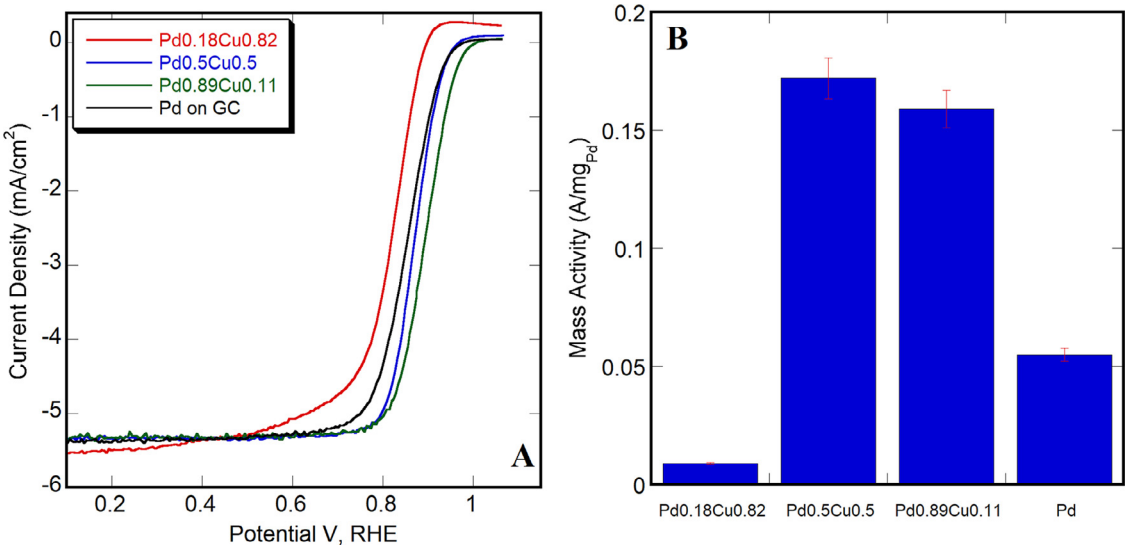

Fig. 4. (A) ORR polarization curves of Pd and Pd-Cu films in 0.1M KOH under 1600 rpm and a scan rate of 10 mV/s, (B) summary of ORR mass activity of Pd and Pd-Cu films at 0.90V vs. RHE.

Table 4
Summary of ECSA of prepared electro-catalysts.

Electrocatalysts	ECSA from H_{UPD} in acidic media (m^2/g_{Pd})	ECSA from CO stripping in acidic media (m^2/g_{Pd})	$ECSA_{CO\_stripping}/ECSA_{HUPD}$
Pd on GC	11.95	12.30	1.03
np $Pd_{0.65}Cu_{0.35}$	34.97	50.86	1.45
np $Pd_{0.37}Cu_{0.63}$	46.98	74.37	1.58

of the as-prepared electrocatalysts. It is seen that the np structures obtained from de-alloying exhibit higher surface area in comparison with the plain Pd film. Also, **Table 4** demonstrates that the np Pd-Cu ECSA from CO stripping is higher than the one obtained by H_{UPD}, whereas the Pd film ECSA from CO stripping is similar to the one from H_{UPD}. This indicates that the Cu in the alloy could truly reduce the amount of underpotentially deposited H atoms similar to the finding reported earlier for the case of Pt-Ni electrocatalysts [34]. In this case of our interest, it would be more accurate to use ECSA from CO stripping to determine the catalytic activity that is discussed in the next section. In addition, the large ECSA (**Table 4**) of np Pd-Cu (np $Pd_{0.65}Cu_{0.35}$ and np $Pd_{0.37}Cu_{0.63}$) films indicate the presence of more active sites for the ORR catalysis application. As shown in Fig. 3**B**, there is a negative shift of the CO stripping peak of np Pd-Cu (green and blue curves) films in comparison with the CO stripping curve (red) of the plain Pd layer. Such a shift indicates a weak bonding between CO and Pd sites in the alloy films. That weak CO bonding is associated with a downshift of the Pd d-band center which has also been suggested in the literature by previous studies [35,36]. CO stripping experiments were also performed in alkaline media (0.1M KOH) as shown in SI **Fig. S4B**. Similarly to the CO stripping in an acidic environment (Fig. 3**B**), the np Pd-Cu electrocatalysts show the negative shift of stripping peak in comparison with Pd on GC. It noteworthy that the CO stripping of all prepared electrocatalysts took place at lower potential compared with the one in acidic media (converted to RHE as showed in SI

Table S1). This observation is consistent with previous literature reports [37,38]. The weak CO bonding with the Pd-Cu active centers in the alloy renders the catalyst a more CO tolerant character, which is beneficial for fuel cell application.

3.4. ORR Performance of Pd-Cu films

The as-deposited Pd-Cu films in this work were tested firstly as electrocatalysts for the ORR in oxygen saturated 0.1 M KOH for comparison purpose. Fig. 4**A** shows the LSV on said films with different compositions held in RDE configuration at 1600 rpm. Previous studies indicate that diffusion limit current density (j_d) should be close to -5.5 mA/cm^2 for a 4 e$^-$ process reduction of O_2 to OH^- [39]. Applying Eq. (3) to our results yields about -5.6 mA/cm^2 for j_d. The slight discrepancy is mostly due to the choice of constant in the equation. Most of the Pd-Cu films exhibit a j_d of about -5.5 mA/cm^2, at 0.6 V vs RHE except the $Pd_{0.18}Cu_{0.82}$ which shows a j_d that is lower than the theoretical value (-5.5 mA/cm^2). This indicates a contribution of a 2e$^-$ process, most likely a partial reduction of O_2 to H_2O_2. Following a standardized procedure in the literature [40] the ORR kinetic current of all Pd-Cu catalysts in this work was calculated by using the Koutecky–Levich equation (Eq. (2)) at a potential of 0.90 V vs. RHE. The mass activity of prepared films was estimated by dividing the kinetic current by the mass of Pd. The results are summarized in the bar graph presented in Fig. 4**B**. A look at these results suggests that the $Pd_{0.50}Cu_{0.50}$ catalyst features the highest mass activity which is around three-times higher than that of a plain Pd film. With the increase of Cu content (as in $Pd_{0.18}Cu_{0.82}$), the respective catalysts show low ORR activity. At the same time, with the Pd content increase (as in $Pd_{0.89}Cu_{0.11}$), the catalytic mass activity was also found to be lower. Overall, this ORR activity trend for as-deposited Pd-Cu films with different compositions is similar to trends observed in previous studies reporting the highest ORR catalytic activity close to 1:1 Pd:Cu ratio [41].

3.5. ORR activity of np Pd-Cu

After investigating the ORR performance of the as-deposited Pd-Cu films, the catalytic performance of np Pd-Cu films was also assessed by LSV in oxygen saturated 0.1 M KOH at 1600 rpm. Fig. 5**A** presents the LSV curves, the half-wave potential of np Pd-Cu and Pd film (Pd electrodeposited on $Pd_{0.37}Cu_{0.63}$ (0.896 V vs. RHE) to be 45 mV and 42 mV, respectively, shifted positively in comparison with the plain Pd film on GC catalyst. In comparison with commercial Pd/C, the half-wave potentials of np $Pd_{0.65}Cu_{0.35}$ and np $Pd_{0.37}Cu_{0.63}$ still show 9 mV and 6 mV positive shift, respectively. In addition, the half-wave potential of the np electrocatalysts in this work is more positive than the precursor Pd-Cu films (shown in Fig. 4**A**) which indicates an enhanced ORR activity. The mass activity and specific activity were calculated by using Eq. (2) to determine the kinetic current at a potential of 0.9 V vs. RHE. The calculated kinectic current is then divided by the total mass of Pd or Pd ECSA from CO stripping. Fig. 5**B** shows the mass activity and specific activity of Pd on GC, np $Pd_{0.65}Cu_{0.35}$, and np $Pd_{0.37}Cu_{0.63}$. The np $Pd_{0.36}Cu_{0.64}$ has the highest both mass activity (1.11A/mg$_{Pd}$) and specific activity (1.42mA/cm$^2_{Pd}$) which is around 22-times and 3-times higher, respectively, than that of the Pd film on GC. In addition, the np $Pd_{0.37}Cu_{0.63}$ shows 6.2-times higher mass activity than that of commercial Pd/C electrocatalysts. It should be noted that for the sake of the most conservative estimation, no iR correction was applied in either of the LSV curves or catalytic activity calculation. Apparently, the np $Pd_{0.37}Cu_{0.63}$ catalyst shows the best ORR activity among all Pd-Cu electrocatalysts reported before (see all results summarized in the **SI Table S2**). The Tafel plots of Pd on GC, np $Pd_{0.65}Cu_{0.35}$ and np $Pd_{0.37}Cu_{0.63}$ are presented in Fig. 5**C**.

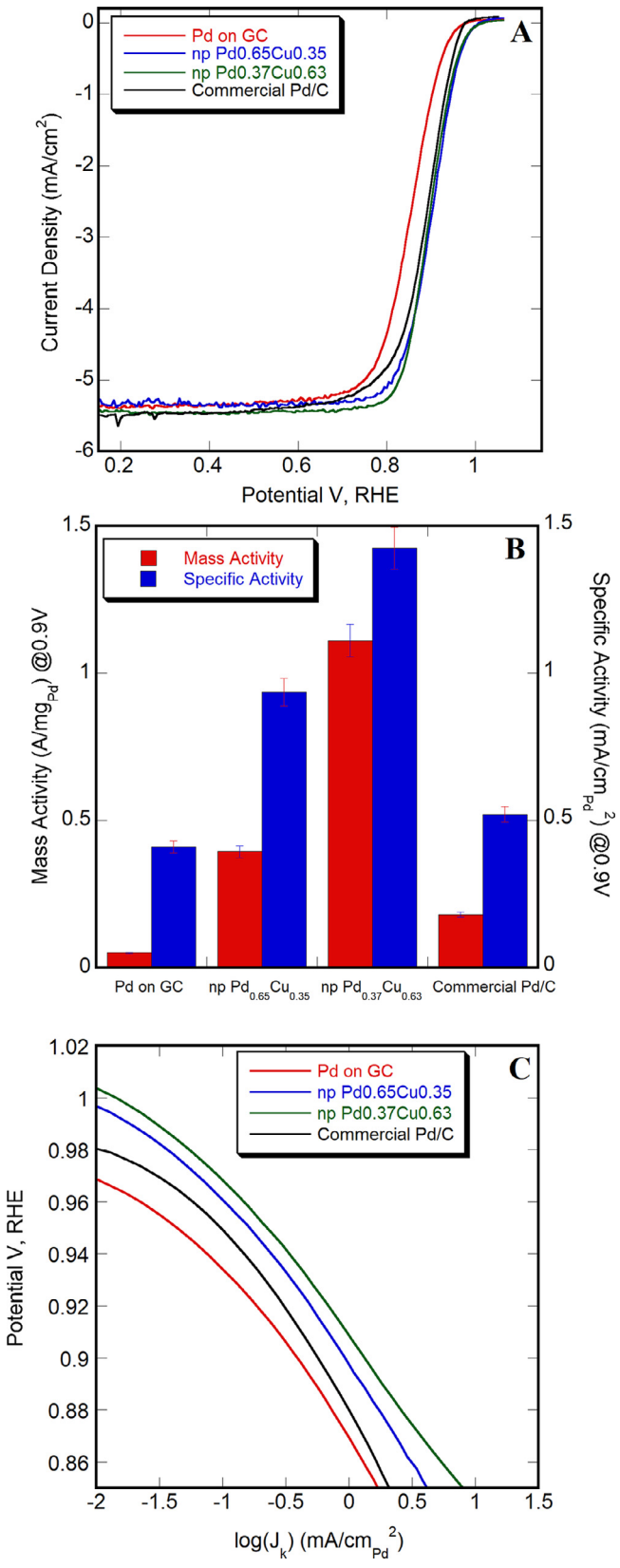

Fig. 5. (A) ORR polarization curves of Pd on GC, np $Pd_{0.65}Cu_{0.35}$ and np $Pd_{0.37}Cu_{0.63}$ in 0.1M KOH under 1600 rpm and a scan rate of 10 mV/s, (B) Mass activity and specific activity of Pd on GC, np $Pd_{0.65}Cu_{0.35}$ and np $Pd_{0.37}Cu_{0.63}$ at 0.90V vs. RHE (C) Tafel plot for Pd on GC, np $Pd_{0.65}Cu_{0.35}$ and np $Pd_{0.37}Cu_{0.63}$.

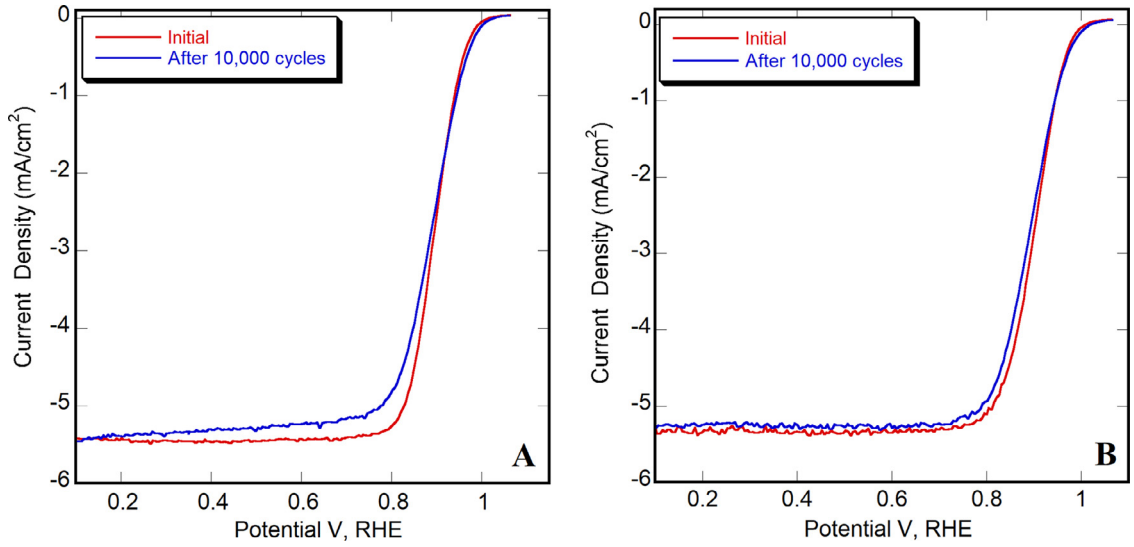

Fig. 6. (A) ORR polarization curves of np $Pd_{0.37}Cu_{0.63}$ before and after 10,000 ADT cycles (B) ORR polarization curves of np $Pd_{0.65}Cu_{0.35}$ before and after 10,000 ADT cycles in 0.1M KOH.

The Tafel slopes of np $Pd_{0.65}Cu_{0.35}$ and np $Pd_{0.37}Cu_{0.63}$ are about -60 mV/dec and -58 mV/dec at low overpotential region ($log(J_k)$ = -0.5), while the Pd on GC and commercial Pd/C catalyst exhibits a Tafel slope of -63 mV/dec and -67 mV/dec at low overpotential region ($log(J_k)$ = -0.5). The lower Tafel slope values of both np $Pd_{0.65}Cu_{0.35}$ and np $Pd_{0.37}Cu_{0.63}$ catalysts indicate a relatively faster reaction rate in comparison with the plain Pd on GC catalyst [42,43]. The smaller Tafel slope is desirable as a smaller change in the applied voltage will lead to a larger increase in the reaction rate [44]. It could be expected that the ORR mechanism is identical for all three electrocatalysts (Pd on GC, np $Pd_{0.65}Cu_{0.35}$ and np $Pd_{0.37}Cu_{0.63}$) due to the similar Tafel slope value [42]. The excellent activity of np $Pd_{0.65}Cu_{0.35}$ and np $Pd_{0.37}Cu_{0.63}$ could be due to the following reasons. Firstly, the fine porous structure is associated with a high surface area (ECSA of Pd as indicated in **Table 4**) which could provide ample Pd active sites for ORR. In addition, the residual Cu entrapped inside the nanoporous structure (**SI** Fig. **S3**) could influence and thus modify the electronic structure of Pd. To achieve maximum ORR activity, Pd needs to be combined with transition metal(s) for establishing a balance between the binding strength of oxygenated species on one hand and the dissociative functionality upon O_2 adsorption on the other [45,46]. Simulation results in the literature indicated that the alloying of Pd with Cu will down-shift the d-band center of Pd and thus facilitating the ORR kinetics [25,26]. The CO stripping technique could be used to indirectly probe the electronic structure of Pd [36,47]. In this work, both np $Pd_{0.65}Cu_{0.35}$ and np $Pd_{0.37}Cu_{0.63}$ feature more negative CO stripping potentials in comparison with Pd on GC (Fig. 3**B**), which implies a downshift of the Pd d-band center. If the d-band center up-shifts to move closer to Fermi level (for plain Pd), the oxygenated species adsorb strongly on the Pd surface which results in poorer ORR activity [45]. In our case of Cu-modified Pd surface, the Pd d-band center is expected to downshift which eventually favors the ORR as the adsorption of oxygenated species becomes weaker [35,48,49].

3.6. ORR durability

To assess the durability of all np Pd-Cu catalysts in this work, accelerated durability tests (ADT) of 10,000 potential cycles were conducted at a scan rate of 100 mV/s in O_2 saturated 0.1 M KOH solution over a potential region between 0.6 V to 1.0 V vs. RHE. Fig. 6**A and** 6**B** present the LSV curves of np $Pd_{0.37}Cu_{0.63}$ and np $Pd_{0.65}Cu_{0.35}$ before and after the ADT testing. The half-wave potentials of both np $Pd_{0.37}Cu_{0.63}$ and np $Pd_{0.65}Cu_{0.35}$ exhibit nearly negligible negative shifts of 5 mV and 4 mV, respectively, after 10,000 ADT cycles. In terms of mass activity, the np $Pd_{0.37}Cu_{0.63}$ features a decay of 9.7%, whereas the np $Pd_{0.65}Cu_{0.35}$ features a 19.7% decrease after 10,000 ADT cycles **(SI Fig. S5).** The decrease of catalytic activity of np Pd-Cu films could be due to the lower Cu (more) stability at the high potential region as stipulated by the Cu Pourbaix diagram [14]. In summary, the np $Pd_{0.37}Cu_{0.63}$ shows excellent durability with only a 9.7% decrease in mass activity, which is promising for alkaline fuel cell application.

4. Conclusions

The np Pd-Cu films synthesized by electrochemical de-alloying of pre-deposited Pd-Cu alloys were used as electrocatalysts for ORR in alkaline media. The nanoporous (np) structure features well-developed ECSA as confirmed by SEM, H_{UPD}, and CO stripping characterizations. The np Pd-Cu electrocatalysts exhibit a high catalytic activity of up to 1.11A/mg_{Pd} at 0.9V vs. RHE and excellent durability with only a negligible decrease of half-wave potential after 10,000 cycles of ADT. The improved catalytic performance of np Pd-Cu could be due to the unique nanoporous structure emphasizing both a high Pd ECSA and an electronic structure modification of Pd by the residual Cu leading to a favorable d-band shift. Further studies will be conducted in the future to understand the relationship between the ORR mechanism and np Pd-Cu electrocatalysts of different compositions and porosity length scales to design electrocatalysts for boosting further the ORR in alkaline media. The nanoporous structure fabricated by a thin film de-alloying clearly demonstrates the advantages of facile electrocatalyst's synthesis and its suitability in fuel cell applications. This de-alloying method could be extended to the design and fabrication of other np electrocatalysts (such as np Pt-Cu, np Pt-Ni, np Ag-Cu, etc) for other reactions, to maximize utilization of noble metals.

Declaration of Competing Interest

The authors declare that they have no known competing financial interests or personal relationships that could have appeared to influence the work reported in this paper.

Credit authorship contribution statement

Yunxiang Xie: Conceptualization, Methodology, Resources, Data curation, Validation, Investigation, Visualization, Writing - original draft, Writing - review & editing. **Can Li:** Methodology, Resources, Validation, Writing - review & editing. **Ezer Castillo:** Resources, Data curation, Writing - review & editing. **Jiye Fang:** Supervision, Funding acquisition, Project administration, Writing - review & editing. **Nikolay Dimitrov:** Supervision, Conceptualization, Visualization, Project administration, Funding acquisition, Writing - review & editing.

Acknowledgments

This work was primarily supported by the Center for Alkaline-Based Energy Solutions, an Energy Frontier Research Center program supported by the US Department of Energy, under Grant DE-SC0019445. Y.X. was also partially supported by the Shimadzu Summer Fellowship at the Department of Chemistry. C.L. was supported by the National Science Foundation (DMR 1808383). SEM/EDX measurements were partially supported by S3IP, State University of New York at Binghamton.

Supplementary materials

Supplementary material associated with this article can be found, in the online version, at doi:10.1016/j.electacta.2021.138306.

References

[1] M.H. Rashid, Power Electronics Handbook, Butterworth-Heinemann, 2017.
[2] B.C. Steele, A. Heinzel, in: Materials for Fuel-Cell Technologies, Materials For Sustainable Energy: A Collection of Peer-Reviewed Research and Review Articles from, Nature Publishing Group, 2011, pp. 224–231. World Scientific.
[3] F.T. Wagner, B. Lakshmanan, M.F. Mathias, Electrochemistry and the future of the automobile, J. Phys. Chem. Lett. 1 (2010) 2204–2219.
[4] S. Gottesfeld, D.R. Dekel, M. Page, C. Bae, Y. Yan, P. Zelenay, Y.S. Kim, Anion exchange membrane fuel cells: current status and remaining challenges, J. Power Sources 375 (2018) 170–184.
[5] T.J. Omasta, A.M. Park, J.M. LaManna, Y. Zhang, X. Peng, L. Wang, D.L. Jacobson, J.R. Varcoe, D.S. Hussey, B.S. Pivovar, Beyond catalysis and membranes: visualizing and solving the challenge of electrode water accumulation and flooding in AEMFCs, Energy Environ. Sci. 11 (2018) 551–558.
[6] A. Sarapuu, E. Kibena-Poldsepp, M. Borghei, K. Tammeveski, Electrocatalysis of oxygen reduction on heteroatom-doped nanocarbons and transition metal-nitrogen-carbon catalysts for alkaline membrane fuel cells, J. Mater. Chem. A 6 (2018) 776–804.
[7] M.K. Debe, Electrocatalyst approaches and challenges for automotive fuel cells, Nature 486 (2012) 43–51.
[8] X. Ge, A. Sumboja, D. Wuu, T. An, B. Li, F.T. Goh, T.A. Hor, Y. Zong, Z. Liu, Oxygen reduction in alkaline media: from mechanisms to recent advances of catalysts, ACS Catal. 5 (2015) 4643–4667.
[9] G. Bampos, L. Sygellou, S. Bebelis, Oxygen reduction reaction activity of Pd-based bimetallic electrocatalysts in alkaline medium, Catal. Today 355 (2020) 685–697.
[10] M. Lüsi, H. Erikson, M. Merisalu, M. Rähn, V. Sammelselg, K. Tammeveski, Electrochemical reduction of oxygen in alkaline solution on Pd/C catalysts prepared by electrodeposition on various carbon nanomaterials, J. Electroanal. Chem. 834 (2019) 223–232.
[11] M. Lüsi, H. Erikson, A. Treshchalov, M. Rähn, M. Merisalu, A. Kikas, V. Kisand, V. Sammelselg, K. Tammeveski, Oxygen reduction reaction on Pd nanocatalysts prepared by plasma-assisted synthesis on different carbon nanomaterials, Nanotechnology 32 (2020) 035401.
[12] X. Peng, T.J. Omasta, J.M. Roller, W.E. Mustain, Highly active and durable Pd-Cu catalysts for oxygen reduction in alkaline exchange membrane fuel cells, Front. Energy 11 (2017) 299–309.
[13] H. Erikson, A. Sarapuu, J. Solla-Gullón, K. Tammeveski, Recent progress in oxygen reduction electrocatalysis on Pd-based catalysts, J. Electroanal. Chem. 780 (2016) 327–336.
[14] B. Beverskog, I. Puigdomenech, Revised Pourbaix diagrams for copper at 25 to 300 C, J. Electrochem. Soc. 144 (1997) 3476.
[15] H. Erikson, A. Kasikov, C. Johans, K. Kontturi, K. Tammeveski, A. Sarapuu, Oxygen reduction on Nafion-coated thin-film palladium electrodes, J. Electroanal. Chem. 652 (2011) 1–7.
[16] Y. Wang, D. Sun, T. Chowdhury, J.S. Wagner, T.J. Kempa, A.S. Hall, Rapid room-temperature synthesis of a metastable ordered intermetallic electrocatalyst, J. American Chem. Soc. 141 (2019) 2342–2347.
[17] X. Lu, M. Ahmadi, F.J. DiSalvo, H.D. Abruña, Enhancing the electrocatalytic activity of Pd/M (M= Ni, Mn) nanoparticles for the oxygen reduction reaction in alkaline media through electrochemical dealloying, ACS Catal. 10 (2020) 5891–5898.
[18] Y. Xie, Y. Yang, D.A. Muller, H.D. Abruña, N. Dimitrov, J. Fang, Enhanced ORR kinetics on Au-doped Pt–Cu porous films in alkaline media, ACS Catal. 10 (2020) 9967–9976.
[19] Y. Xie, N. Dimitrov, Ultralow Pt loading nanoporous Au-Cu-Pt thin film as highly active and durable catalyst for formic acid oxidation, Appl. Catal. B Environ. 263 (2020) 118366.
[20] P. Mukherjee, P.S. Roy, K. Mandal, D. Bhattacharjee, S. Dasgupta, S.K. Bhattacharya, Improved catalysis of room temperature synthesized Pd-Cu alloy nanoparticles for anodic oxidation of ethanol in alkaline media, Electrochim. Acta 154 (2015) 447–455.
[21] M. Lusi, H. Erikson, M. Merisalu, A. Kasikov, L. Matisen, V. Sammelselg, K. Tammeveski, Oxygen Electroreduction in Alkaline Solution on Pd Coatings Prepared by Galvanic Exchange of Copper, Electrocatal. Us 9 (2018) 400–408.
[22] R. Newman, K. Sieradzki,, F.U. Renner, A. Hodge, J. Balk, J.W. Kysar, O. Okman, Y. Ding, H. Ma, J. Weissmüller, Nanoporous Gold: From An Ancient Technology to a High-tech Material, Royal Society of Chemistry, 2012.
[23] T. Fujita, P. Guan, K. McKenna, X. Lang, A. Hirata, L. Zhang, T. Tokunaga, S. Arai, Y. Yamamoto, N. Tanaka, Atomic origins of the high catalytic activity of nanoporous gold, Nature Mater. 11 (2012) 775–780.
[24] X. Wang, W. Wang, Z. Qi, C. Zhao, H. Ji, Z. Zhang, Fabrication, microstructure and electrocatalytic property of novel nanoporous palladium composites, J. Alloys Compounds 508 (2010) 463–470.
[25] M.V. Castegnaro, W.J. Paschoalino, M.R. Fernandes, B. Balke, M.C.M. Alves, E.A. Ticianelli, J. Morais, Pd–M/C (M= Pd, Cu, Pt) Electrocatalysts for Oxygen reduction reaction in alkaline medium: correlating the electronic structure with activity, Langmuir 33 (2017) 2734–2743.
[26] U.B. Demirci, Theoretical means for searching bimetallic alloys as anode electrocatalysts for direct liquid-feed fuel cells, J. Power Sources 173 (2007) 11–18.
[27] A. Correia, L. Mascaro, S. Machado, L. Avaca, Active surface area determination of Pd-Si alloys by H-adsorption, Electrochim. Acta 42 (1997) 493–495.
[28] J. Soto-Hernández, C. Santiago-Ramirez, E. Ramirez-Meneses, M. Luna-Trujillo, J.-A. Wang, L. Lartundo-Rojas, A. Manzo-Robledo, Electrochemical reduction of NOx species at the interface of nanostructured Pd and PdCu catalysts in alkaline conditions, Appl. Catal. B Environ. 259 (2019) 118048.
[29] J. Koutecky, B. Levich, The application of the rotating disc electrode to studies of kinetic and catalytic processes, Zhurnal Fizicheskoi Khimii 32 (1958) 1565–1575.
[30] T. Xia, J. Liu, S. Wang, C. Wang, Y. Sun, L. Gu, R. Wang, Enhanced catalytic activities of NiPt truncated octahedral nanoparticles toward ethylene glycol oxidation and oxygen reduction in alkaline electrolyte, ACS Appl. Mater. Interf. 8 (2016) 10841–10849.
[31] C. Milhano, D. Pletcher, The electrodeposition and electrocatalytic properties of copper–palladium alloys, J. Electroanal. Chem. 614 (2008) 24–30.
[32] J. Erlebacher, M.J. Aziz, A. Karma, N. Dimitrov, K. Sieradzki, Evolution of nanoporosity in dealloying, Nature 410 (2001) 450–453.
[33] S.N. Pronkin, A. Bonnefont, P.S. Ruvinskiy, E.R. Savinova, Hydrogen oxidation kinetics on model Pd/C electrodes: Electrochemical impedance spectroscopy and rotating disk electrode study, Electrochim. Acta 55 (2010) 3312–3323.
[34] D.F. van der Vliet, C. Wang, D. Li, A.P. Paulikas, J. Greeley, R.B. Rankin, D. Strmcnik, D. Tripkovic, N.M. Markovic, V.R. Stamenkovic, Unique electrochemical adsorption properties of Pt-Skin Surfaces, Angewandte Chemie 124 (2012) 3193–3196.
[35] J. Liu, X. Fan, C.Q. Sun, W. Zhu, DFT study on intermetallic Pd–Cu alloy with cover layer Pd as efficient catalyst for oxygen reduction reaction, Materials 11 (2018) 33.
[36] M.T. Gorzkowski, A. Lewera, Probing the limits of d-band center theory: electronic and electrocatalytic properties of Pd-shell–Pt-core nanoparticles, J. Phys. Chem. C 119 (2015) 18389–18395.
[37] N.M. Markovic, C.A. Lucas, A. Rodes, V. Stamenkovi, P.N. Ross, Surface electrochemistry of CO on Pt(111): anion effects, Surface Sci. 499 (2002) L149–L158.
[38] J.S. Spendelow, G.Q. Lu, P.J.A. Kenis, A. Wieckowski, Electrooxidation of adsorbed CO on Pt(111) and Pt(111)/Ru in alkaline media and comparison with results from acidic media, J. Electroanal. Chem. 568 (2004) 215–224.
[39] Y. Yang, G. Chen, R. Zeng, A.M. Villarino, F.J. DiSalvo, R.B. van Dover, H.D. Abruña, Combinatorial studies of palladium-based oxygen reduction electrocatalysts for alkaline fuel cells, J. Am. Chem. Soc. 142 (2020) 3980–3988.
[40] C. Campos-Roldán, R. González-Huerta, N. Alonso-Vante, Experimental protocol for HOR and ORR in alkaline electrochemical measurements, J. Electrochem. Soc. 165 (2018) J3001.
[41] W. Tang, L. Zhang, G. Henkelman, Catalytic activity of Pd/Cu random alloy nanoparticles for oxygen reduction, J. Phys. Chem. Lett. 2 (2011) 1328–1331.
[42] A. Holewinski, S. Linic, Elementary mechanisms in electrocatalysis: revisiting the ORR Tafel slope, J. Electrochem. Soc. 159 (2012) H864.
[43] S. Fletcher, Tafel slopes from first principles, J. Solid State Electrochem. 13 (2009) 537–549.
[44] E. Gileadi, Physical Electrochemistry: Fundamentals, Techniques and Applications, Wiley-VCH, Weinheim, 2011.

[45] T. Gunji, R.H. Wakabayashi, S.H. Noh, B. Han, F. Matsumoto, F.J. DiSalvo, H.D. Abruña, The effect of alloying of transition metals (M= Fe, Co, Ni) with palladium catalysts on the electrocatalytic activity for the oxygen reduction reaction in alkaline media, Electrochim. Acta 283 (2018) 1045–1052.
[46] W. Tang, G. Henkelman, Charge redistribution in core-shell nanoparticles to promote oxygen reduction, J Chem. Phys. 130 (2009) 194504.
[47] S. Hu, F. Munoz, J. Noborikawa, J. Haan, L. Scudiero, S. Ha, Carbon supported Pd-based bimetallic and trimetallic catalyst for formic acid electrochemical oxidation, Appl. Catal. B Environ. 180 (2016) 758–765.
[48] B. Hammer, J. Nørskov, Electronic factors determining the reactivity of metal surfaces, Surface Sci. 343 (1995) 211–220.
[49] M. Mavrikakis, B. Hammer, J.K. Nørskov, Effect of strain on the reactivity of metal surfaces, Phys. Rev. Lett. 81 (1998) 2819.